Structural Basis of Reversible Phosphorylation by Maize Pyruvate Orthophosphate Dikinase Regulatory Protein[1][OPEN]

Lun Jiang[2], Yi-bo Chen[2], Jiangge Zheng, Zhenhang Chen, Yujie Liu, Ye Tao, Wei Wu, Zhongzhou Chen*, and Bai-chen Wang*

State Key Laboratory of Agrobiotechnology, China Agricultural University, Beijing 100193, China (L.J., J.Z., Zhenhang Chen, Y.L., W.W., Zhongzhou Chen); Photosynthesis Research Center, Key Laboratory of Photobiology, Institute of Botany, Chinese Academy of Sciences, Xiangshan, Beijing 100093, China (Y.-B.C., B.-C.W.); and Beijing Synchrotron Radiation Facility, Institute of High Energy Physics, Chinese Academy of Sciences, Beijing 100049, China (Y.T.)

ORCID ID: 0000-0003-1319-9664 (Z.C.).

Pyruvate orthophosphate dikinase (PPDK) is one of the most important enzymes in C_4 photosynthesis. PPDK regulatory protein (PDRP) regulates the inorganic phosphate-dependent activation and ADP-dependent inactivation of PPDK by reversible phosphorylation. PDRP shares no significant sequence similarity with other protein kinases or phosphatases. To investigate the molecular mechanism by which PDRP carries out its dual and competing activities, we determined the crystal structure of PDRP from maize (*Zea mays*). PDRP forms a compact homo-dimer in which each protomer contains two separate N-terminal (NTD) and C-terminal (CTD) domains. The CTD includes several key elements for performing both phosphorylation and dephosphorylation activities: the phosphate binding loop (P-loop) for binding the ADP and inorganic phosphate substrates, residues Lys-274 and Lys-299 for neutralizing the negative charge, and residue Asp-277 for protonating and deprotonating the target Thr residue of PPDK to promote nucleophilic attack. Surprisingly, the NTD shares the same protein fold as the CTD and also includes a putative P-loop with AMP bound but lacking enzymatic activities. Structural analysis indicated that this loop may participate in the interaction with and regulation of PPDK. The NTD has conserved intramolecular and intermolecular disulfide bonds for PDRP dimerization. Moreover, PDRP is the first structure of the domain of unknown function 299 enzyme family reported. This study provides a structural basis for understanding the catalytic mechanism of PDRP and offers a foundation for the development of selective activators or inhibitors that may regulate photosynthesis.

In C_4 plants, pyruvate orthophosphate dikinase (PPDK), which catalyzes the reversible phosphorylation of pyruvate to phospho*enol*pyruvate, is the most important rate-limiting C_4 cycle enzyme (Edwards et al., 1985). Phosphorylation and dephosphorylation of residue Thr-527 of PPDK lead to its inactivation and activation, respectively. This process is accomplished by a single, bifunctional protein, namely PPDK regulatory protein (PDRP; Burnell and Hatch, 1985), and the process is light intensity dependent (Hatch and Slack, 1969; Chen et al., 2014b). PDRP is an unusual enzyme in three respects. First, PDRP is a bifunctional enzyme that catalyzes both phosphorylation and dephosphorylation, and these activities are usually catalyzed by separate kinases and phosphatases. Second, PDRP uses ADP as the phosphoryl donor for kinase activity, while most kinases utilize ATP. Third, unlike most phosphatases that dephosphorylate substrates to yield inorganic phosphate (Pi), PDRP employs a Pi-dependent, pyrophosphate (PPi)-forming dephosphorylation mechanism (Ashton et al., 1984).

Owing to the importance in regulating C_4 photosynthetic cycle, the preliminary studies on maize (*Zea mays*) PDRP carried out in the 1980s were widely considered to represent a significant breakthrough in the field of C_4 photosynthesis research. Burnell and Hatch (1983) identified PDRP as a regulator of PPDK. They used in vitro activity assays to detect the reversible phosphorylation of PPDK by PDRP (Burnell and Hatch, 1985). By selectively substituting Ser or Tyr for the targeted Thr residue in the active site of PPDK, Chastain et al. (2000) discovered that Ser but not Tyr was functionally

[1] This work was supported by the State Key Program of National Natural Science of China (grant no. 31030017), National Natural Science Foundation of China (grant nos. 31222032 and 31370720), and Extramural Scientists of State Key Laboratory of Agrobiotechnology (2016SKLAB6-1).

[2] These authors contributed equally to the article.

* Address correspondence to chenzhongzhou@cau.edu.cn or wangbc@ibcas.ac.cn.

The author responsible for distribution of materials integral to the findings presented in this article in accordance with the policy described in the Instructions for Authors (www.plantphysiol.org) is: Zhongzhou Chen (chenzhongzhou@cau.edu.cn) or Bai-chen Wang (wangbc@ibcas.ac.cn).

L.J. and Y.-B.C. performed the gene cloning, protein expression, purification, and assay; L.J. carried out crystallization, the diffraction data collection, and structure determination; all authors contributed to the experimental design, data analysis, and discussion; L.J., B.-C.W. and Z.C. conceived the project and wrote the article.

[OPEN] Articles can be viewed without a subscription.

www.plantphysiol.org/cgi/doi/10.1104/pp.15.01709

similar to the Thr residue (Chastain et al., 2000). This led to the conclusion that PDRP was a member of the Ser/Thr family of protein kinases (Scheeff and Bourne, 2005).

Unfortunately, extensive studies on PDRP have been hindered by the low protein abundance in vivo and difficult protein purification in vitro, and our understanding of the mechanism of the dual enzymatic activities was not significantly advanced. More recently, PDRP was cloned from both maize and Arabidopsis (*Arabidopsis thaliana*), and bioinformatics analysis only predicted a phosphate binding loop (P-loop) domain and a conserved domain of unknown function 299 (DUF299) domain (Burnell and Chastain, 2006; Chastain et al., 2008). Moreover, multiple sequence alignment and molecular phylogenetic analysis has indicated that PDRP from many species appears to lack a canonical protein kinase subdomain and defined protein phosphatase motifs, and the PDRPs of plants may belong to the DUF 299 family (Chastain et al., 2008). Surprisingly, a DUF299 of *Escherichia coli* regulates the reversible phosphorylation of the target Thr residue in the active site of PEP synthetase (PEPS, homolog of PPDK), and the process is also ADP and Pi dependent just as is maize PDRP. This DUF299 gene was subsequently established as PSRP (EC 2.7.11.33 and 2.7.4.28), the PEPS regulatory protein (Burnell, 2010). However, the detailed catalytic mechanism of PSRP, as with PDRP, has remained obscure.

It is also unclear whether PDRP uses two separate or one shared active site to perform phosphorylation and dephosphorylation activities. Differential effects on the enzymatic activities in thermolysin studies indicated two separate sites (Burnell and Hatch, 1986). However, the respective inhibition by phosphorylated and nonphosphorylated PPDK suggested that PDRP may contain separate active sites in relatively close proximity (Burnell and Hatch, 1985).

In this study, we determined the crystal structure of PDRP and identified clear electron density corresponding to a bound AMP molecule. Combined structural analysis and enzymatic experiments suggest PDRP uses a single active site to perform both phosphorylation and dephosphorylation activities. Structural alignment and activity assays of site-directed mutagenesis provided comprehensive insight into the evolutionary relationships with other bifunctional protein kinase-phosphatases and the catalytic mechanism that may prove useful for the development of selective activators and inhibitors.

RESULTS

PDRP Is Comprised of Two Separate Domains

Owing to the difficult purification and crystallization as well as the low sequence homology shared with structure-solved proteins, it has been a considerable struggle to solve the first crystal structure of PDRP. Despite the challenges, we have solved the structure of the maize PDRP. The structure consists of residues 42 to 426, lacking the N-terminal 41 residues of the predicted chloroplastic targeting sequence (Emanuelsson et al., 1999; Burnell and Chastain, 2006). Residues 42 to 125, 130 to 134, and 347 to 367 (Supplemental Fig. S1) are not visible in the electron density. The PDRP monomer comprises two separate compact domains: the N-terminal domain (NTD) and the C-terminal domain (CTD), which are connected by a loop (residues 241–259, L-loop). The NTD has a central four-stranded parallel β-sheet (β1–β4) that forms a sandwich structure, and helix α1 packs against the bottom of the β-sheet, while helices α2 and α3 pack against the top (Fig. 1). Helix α4 connects to the CTD. The CTD also has a central four-stranded parallel β-sheet (βA–βD) that forms a similar sandwich structure, with helices αD and αE packing against the top, helices αC and αF packing against the bottom, and helices αA and αB connecting to the NTD (Fig. 1). The P-loop comprising residues G_{293}VSRTGKT_{300} is at the C terminus of βA and extends into αC (Supplemental Movie S1).

During the initial optimization, PDRP crystals diffracted weakly, and we suspected that the loops that are highly flexible may be the main factor. The addition of small molecules such as ligands or inhibitors can lock such flexible loops into a stable conformation to facilitate crystal packing. To this end, considering that PDRP possesses a conserved P-loop, we added various nucleotides to the well solution, and this improved x-ray diffraction to 3.2 Å. Surprisingly, we observed unexpected electron density for AMP in the NTD not the CTD (Figs. 1 and 2D).

The NTD and CTD Share the Same Protein Fold

Although the sequence homology between the NTD and the CTD (excluding the first two α-helices αA and αB) is only 25%, both share the same protein fold by structural alignment. Additionally, the spatial arrangement of the central β-sheet is similar, with β4-β3-β1-β2 (left to right) of the NTD (Fig. 2A) overlapping well with β_D-βC-βA-βB (left to right) of the CTD (Fig. 2B). We also noticed that the second and third α-helices of both the NTD and the CTD pack against one side of the central β-sheet, while the first α-helix packs against the other side. The main difference between the NTD and the CTD is that the fourth α-helix faces opposite directions (comparing α4 with αF; Fig. 2C). Additionally, the position of the first three α-helices differs significantly.

We predicted that the P-loop of the CTD (Fig. 2B) would bind the nucleotide added to the reservoir solution. However, no additional electron density was observed in the vicinity of the P-loop. In contrast and unexpectedly, we observed clear electron density in the omit *2Fo-Fc* map (Fig. 2D) close to loop S_{144}DGTGWT_{150} of the NTD, which is similar to the P-loop of the CTD (Fig. 2C). We therefore termed this region the putative P-loop. The AMP molecule appears to be bound

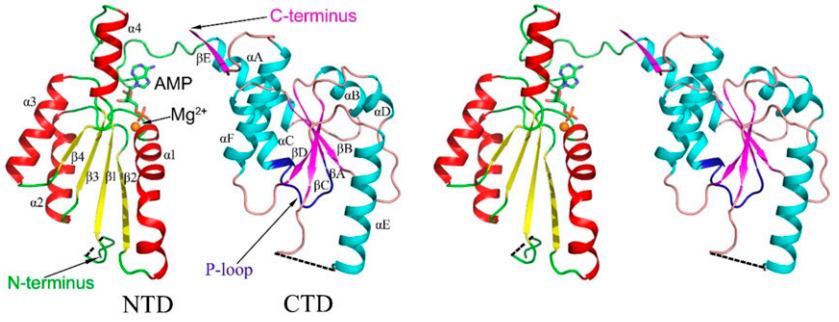

Figure 1. Stereoview of the PDRP structure. The whole structure consists of an NTD, a CTD, and a long linker. The β-sheets and α-helices of the NTD are colored yellow and red, respectively, and magenta and cyan in the CTD, respectively. The P-loop (blue), AMP (green sticks), and Mg^{2+} ion (orange sphere) are shown, and regions missing in the electron density are indicated by black dashed lines.

strongly via multiple hydrogen bonds and salt bridges (Fig. 2E). The phosphate moiety of AMP forms hydrogen bonds with the amide groups of Thr-147, Gly-148, Trp-149, and Thr-150, the guanidine group of Arg-249, and the hydroxyl groups of Ser-144, Thr-147, and Thr-150 (Fig. 2E). The ribose moiety and base group of AMP interact via hydrogen bonds with the main chain amide group of Arg-249, the side chains of Thr-204, and Glu-163′ from the adjacent protomer. The Mg^{2+} ion interacts with the phosphate moiety of AMP via salt bridges. Moreover, AMP interacts with PDRP via numerous van der Waals interactions (Fig. 2E).

Given the evident structural homology between the NTD and the CTD, we suspected that the putative P-loop of the NTD may be one of the two proposed enzymatic active sites of PDRP, or the binding of AMP to the putative P-loop may be an artifact due to crystal packing.

PDRP Is a Homodimer in Vitro

It has been shown previously that maize PDRP exists as a dimer at pH 7.5 and a tetramer at pH 8.3, with the latter likely to be the more active form (Burnell and Hatch, 1985). Interestingly, our analytical gel filtration showed that PDRP mainly exists as a dimer (Supplemental Fig. S2A). Moreover, the oligomerization state did not change across a pH range of 7.5 to 8.3, and sedimentation velocity (SV) results further

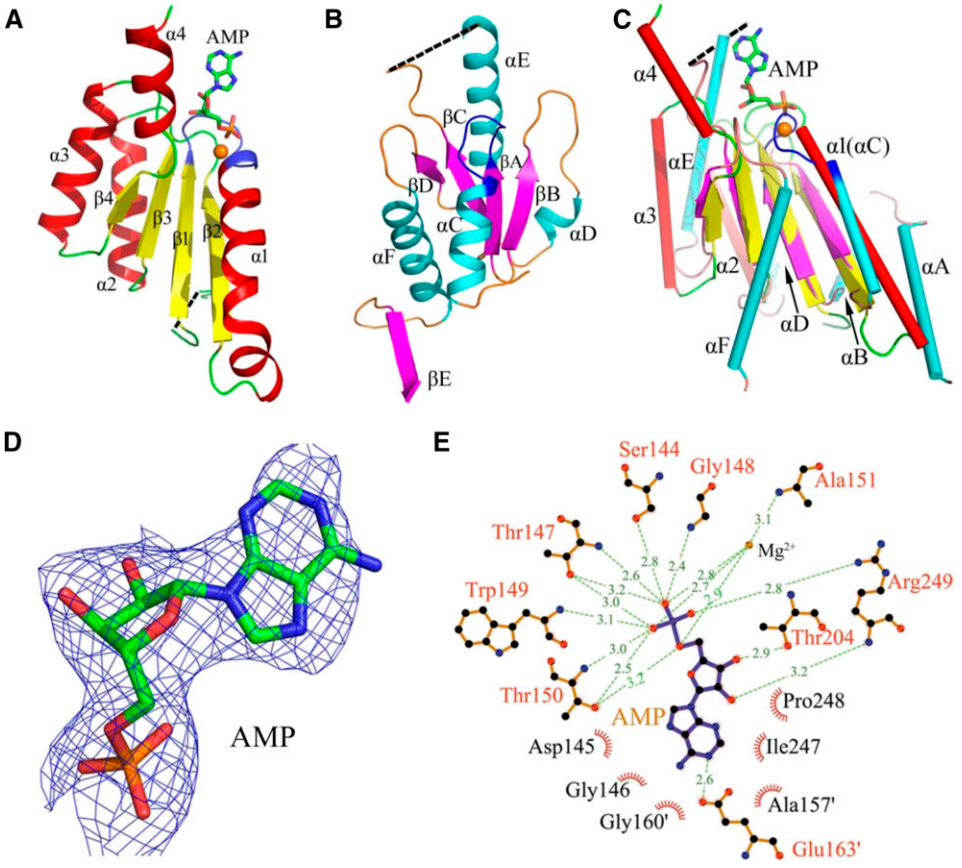

Figure 2. Structures of the NTD and CTD of PDRP. A, Cartoon representation of the NTD of PDRP. B, Cartoon representation of the CTD of PDRP. Both have a central four-stranded parallel β-sheet sandwiched by three to four α-helices. The P-loop and putative P-loop are colored blue. C, Structural alignment between the NTD and CTD. D, The omit *2Fo-Fc* electron density map of bound AMP at the 2.0 σ level. E, Detailed interactions and hydrogen bonds between PDRP and AMP.

confirmed that maize PDRP is dimeric in vitro (Supplemental Fig. S2B).

The PDRP monomer structure resembles a saddle with a concave surface, and the PDRP dimer is largely stabilized by an interlaced network of interactions between the concave surface. The NTDs from the two protomers interact and are stacked at the bottom of the CTDs (Fig. 3A; Supplemental Movie S2). The dimer interface buries 3691 Å^2 of accessible surface area, and dimerization involves numerous hydrogen bonds and salt bridges. We named the loop between αF and βE (residues 415–421) as the interaction loop (I-loop; Fig. 3A; Supplemental Fig. S1). The PDRP protomer contributes three principal separate regions to the dimer interactions. The first is the α1 helix of the NTD from one protomer that is involved in numerous hydrogen bonds with the α1′ helix, L′-loop, and I′-loop from the other protomer. For example, Q161 interacts with residues 245 to 247 of the L′-loop (Fig. 3B), and E163 forms a hydrogen bond with AMP′ from the other protomer (Fig. 2E). The second region involves helix α2 that interacts with the I′-loop via hydrogen bonds and salt bridges. Specifically, Q193 and E197 of helix α2 form hydrogen bonds and salt bridges with S418 and

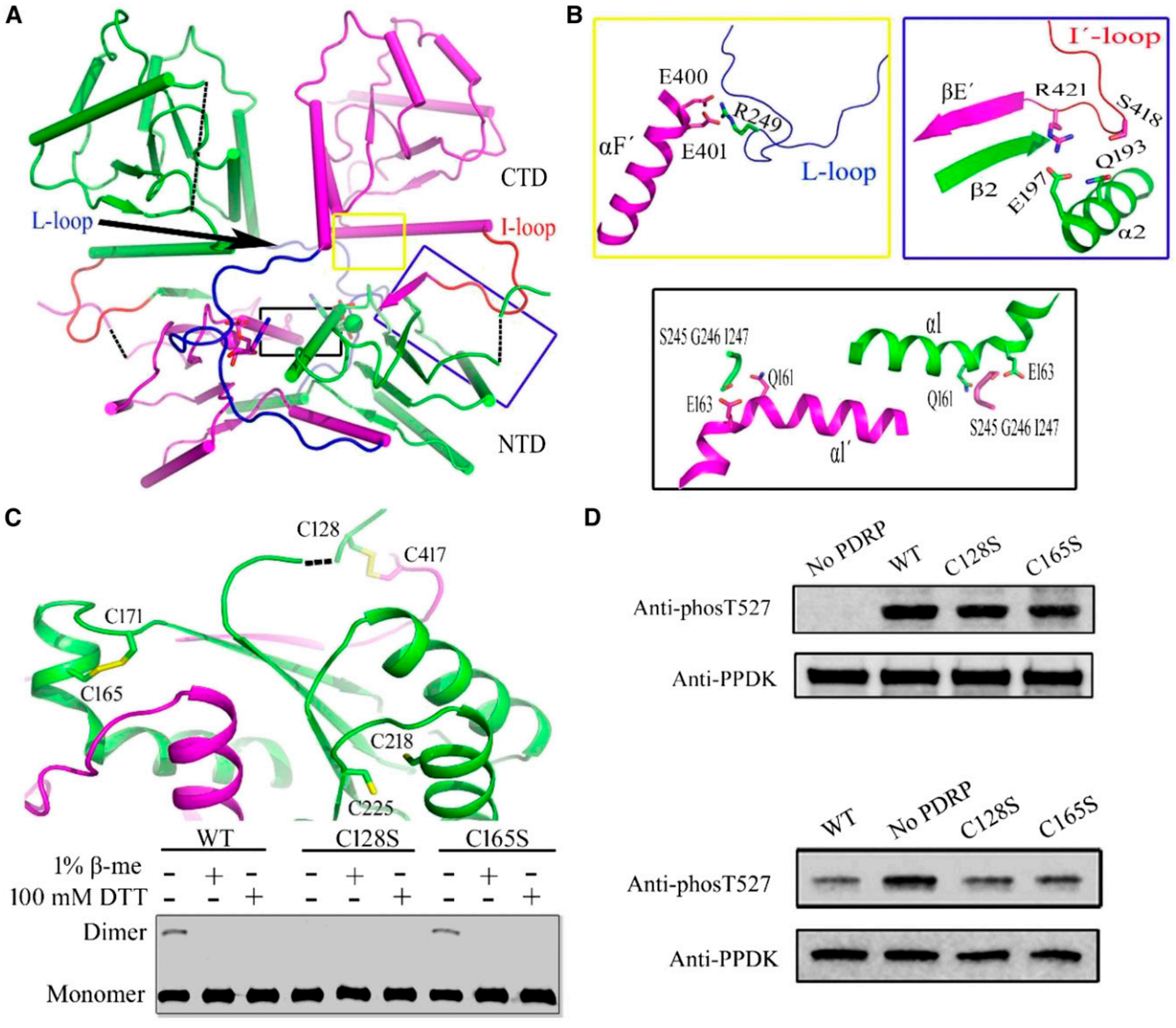

Figure 3. Structure of the PDRP dimer. A, Structural overview of the PDRP dimer, colored by protomers, green and magenta. The L-loop and I-loop are colored blue and red, respectively. The three principal regions involved in dimerization are shown in black, yellow, and blue rectangles. B, Details of the PDRP dimeric interface within the three principal regions. C, Intramolecular (C165-C171) and intermolecular (C128-C417) disulfide bonds are shown in stick representation. In the bottom panel, nine PDRP samples were pretreated with or without reducing agent (1% β-mercaptoethanol or 100 mM DTT) prior to separation by SDS-PAGE. D, Immuno-based assays of the in vitro kinase (top) and pyrophosphorylase (bottom) activities. Western blots were probed with antiphospho-T527-PPDK (antiphosT527) or anti-PPDK antibodies.

R421 of the I′-loop. Interestingly, the β2 sheet forms an antiparallel stranded β-sheet with βE′ from the other protomer (Fig. 3B), thus extending the hydrogen bond network. The third region involves the L-loop, from which R249 forms hydrogen bonds and salt bridges with E400 and E401 of the αF′ helix from the other protomer (Fig. 3B). Taken together, the large interfacial surface area and extensive network of interactions indicate a strong interaction between the two PDRP protomers.

The PDRP Homodimer Has Intramolecular and Intermolecular Disulfide Bonds

Besides the aforementioned hydrogen bonds and salt bridges, dimerization is also stabilized by two intramolecular disulfide bridges between C165 and C171 within each protomer, and two intermolecular disulfide bridges between C128 and C417 of each protomer. These disulfide bonds are relatively flexible, as indicated by the high B-factors (Supplemental Fig. S3B), which may explain the difficulty experienced in reproducibly growing diffracting crystals, even after optimization of the crystallization conditions. We investigated the homogeneity of purified PDRP by pretreatment with or without a reducing agent prior to separation by SDS-PAGE (Fig. 3C), and western blotting showed that both the wild-type protein and the C165S mutant existed in both monomeric and dimeric forms in the absence of a reducing agent and the addition of β-mercaptoethanol or dithiothreitol (DTT) resulted in only the monomer being present. In contrast, the C128S mutant was present only in the monomeric form with or without reducing agent, confirming the C128-C417 intermolecular disulfide bond.

In vitro phosphorylation and dephosphorylation activity assays were performed to investigate the role of the disulfide bridges on the enzymatic activities. It should be noted that the truncated fragment 42-426, referred to as wild type throughout this study, displayed reversible phosphorylation activity on PPDK in vitro (Fig. 3D). The enzymatic activities of the C128S and C165S mutants were comparable with the wild type (Fig. 3D), demonstrating that the disulfide bonds are not involved directly in catalysis.

The CTD Is the Site of Both Kinase and Pyrophosphorylase Activities

To gain insight into the kinase and pyrophosphorylase activities of PDRP, separate DALI searches were performed with the NTD, CTD, and full-length structures. For the NTD, the best match was the amino-terminal domain of the AMPA-sensitive Glu receptor GluA2 (PDB ID 4U5F, residues 6–116; Chen et al., 2014a) with an overall root mean square deviation (rmsd) of 2.7 Å between 94 corresponding C-alpha atoms. Superimposition of the NTD onto GluA2 (Fig. 4A) revealed their similar overall topology and connectivity. Both of them have a central four-stranded parallel β-sheet with the same spatial arrangement packed against one α-helix on one side and two α-helices on the other side forming the characteristic sandwich structure.

In the GluA2 structure, the substrate binds in the central ligand-binding domain between the amino-terminal domain and the transmembrane domain (Dürr et al., 2014). Interestingly, the corresponding part in PDRP is the L-loop. Given the structural similarity between NTD and GluA2, the substrate binding region in PDRP may be assembled from the L-loop and the putative P-loop (Fig. 4A). Excluding GluA2, most of the other DALI hits from the NTD search were protein receptors; we therefore conjectured the substrate binding site in the NTD may function as an allosteric effector

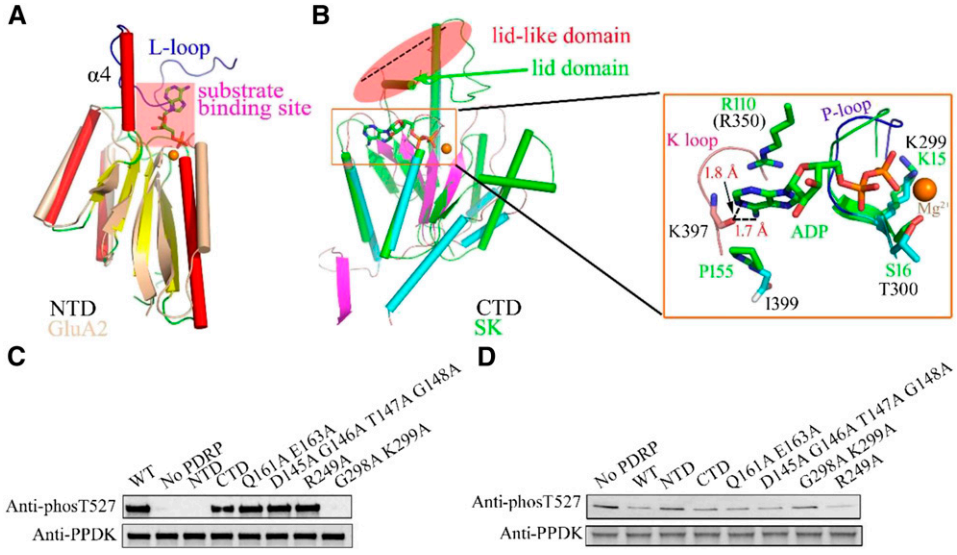

Figure 4. Structural homologs of the NTD and CTD of PDRP. A, Structural alignment between GluA2 (tint, PDB ID 4U5F; Chen et al., 2014a) and the NTD of PDRP. The predicted substrate binding site is indicated by a magenta rectangle. B, Structural alignment between the CTD of PDRP and shikimate kinase (green, PDB ID 1L4Y; Gu et al., 2002). The lid domain of SK is indicated by a green arrowhead, and the corresponding lid-like domain of PDRP is indicated by a red oval. C, Immuno-based assays of the in vitro kinase experiments. D, Immuno-based assays of the in vitro pyrophosphorylase experiments.

that acts to modify the enzymatic activity of PDRP. Alternatively, this part of the structure may mediate protein-protein interactions with PPDK.

Both of the CTD and full-length structures of PDRP gave similar DALI results, so we focused on discussing the results of the CTD search for detail. The CTD showed the highest similarity with shikimate kinase (SK; PDB ID 1L4Y, residues 2–166; Gu et al., 2002), with an rmsd of 2.2 Å between 97 corresponding C-alpha atoms. SK belongs to the nucleoside monophosphate (NMP) kinase family and contains three domains: a core domain containing a P-loop, a lid domain that closes over the bound ATP, and the NMP-binding domain that binds a specific NMP (Gan et al., 2006).

Interestingly, the lid domain is missing in the apo-SK structure, and substrate binding to SK causes a conformational change in the lid domain that becomes ordered and closes over the active site. Similarly, the equivalent lid-like region (residues 346–367) was absent in our PDRP structure (Fig. 4B). Moreover, despite repeated attempts to soak or cocrystallize PDRP with ADP or analogs, we failed to obtain a protein-ligand complex structure. It was suggested that a SO_4^{2-} ion inhibited the binding of AMPPCP to SK (Gan et al., 2006), and it is possible that the MOPS in the crystallization solution prevented the binding of ADP to PDRP in this study. Alternatively, the lid-like domain that is needed to bind ADP may not pack correctly without the PPDK substrate. We did, however, manage to model ADP into the active site of PDRP, and the distance between the N1 nitrogen, 6-amino group of the adenine base and main chain carbonyl of Lys-397 was 1.7 Å and 1.8 Å, respectively (Fig. 4B). To reduce this steric hindrance, the K-loop between βD and αF (residues 394–398) must alter its conformation, and this may explain our failure to obtain a PDRP-ADP complex structure. Interestingly, the cleft between the P-loop, K-loop, and βB is not large enough to incorporate ATP, and this may explain the selectivity for ADP.

We modeled ADP and the Mg^{2+} ion from the SK structure into the PDRP active site to investigate substrate interactions (Fig. 4B). The conserved residues are similar in the respective P-loop structures of PDRP (G_{293}VSRTGKT_{300}) and SK (G_9LPGSGKS_{16}), and given that SK binds directly to ADP, the interactions are likely to exist for PDRP. The side chains of Lys-299 and Lys-15 interact with oxygen atoms of the β-phosphate of ADP, and Thr-300 and Ser-16 directly coordinate the bound Mg^{2+} ion. Besides interacting with the α-phosphate of ADP, Gly-298 and Gly-14 are catalytically important and likely facilitate the essential hinge motion of the P-loop upon binding ADP. The adenine and ribose interactions are also provided by the residues far away from P-loops in sequence. The side chains of Arg-110 and Pro-155 of SK provide direct contacts to the ribose ring, and in the corresponding region of PDRP, Arg-350 in the missing lid-like domain may interact with the ribose ring, while the amide group of Ile-399 contacts the 6-amino group of the adenine base (Fig. 4B).

The results of the DALI searches suggest that the CTD may perform both enzymatic activities, and then we performed in vitro enzymatic experiments to investigate this possibility. A number of dimer interface mutants (R249A, Q161/E163A) exhibited activity comparable with the wild-type protein (Fig. 4, C and D), as observed with the disulfide bond mutants. To investigate whether the putative P-loop in the NTD is involved in the enzymatic activity or not, we mutated all the residues (D_{145}GT_{148}) to Ala, and again the mutations did not affect the catalytic activity. In contrast, mutating residues G298/K299 in the P-loop resulted in the complete loss of enzymatic activity (Fig. 4, C and D). We next engineered and purified separate NTD and CTD, the CTD construct exhibited phosphorylation (Fig. 4C) and dephosphorylation (Fig. 4D) activities that were only slightly lower than the wild-type protein, while the NTD construct was completely devoid of both enzymatic activities. Therefore, the putative P-loop in the NTD appears not to be involved in enzymatic activity, and the bound AMP may be an artifact of crystal packing. However, we cannot exclude the possibility that AMP or other small molecules in vivo may regulate the interaction between PDRP and PPDK via the putative P-loop.

The PDRP Catalytic Mechanism

Although the CTD of PDRP performs both phosphorylation and dephosphorylation activities, the detailed mechanism remains obscure. The DALI search revealed higher similarity with NMP kinases rather than bifunctional kinase-phosphatases for PDRP. We therefore manually searched for other bifunctional kinase-phosphatases to uncover the catalytic mechanism of PDRP.

Structures in the PDB suggest that the bifunctional kinase-phosphatases have evolved a protein scaffold that is capable of binding substrates ranging from nucleotides to metabolic intermediates. Only a small number of dual-activity enzymes act on protein substrates, and of these, His-containing phosphocarrier protein (HPr) kinase/phosphatases (HprK/Ps) from *Staphylococcus xylosus*, *Mycoplasma pneumoniae*, and *Lactobacillus casei* were found to contain the typical P-loop required to catalyze reversible phosphorylation of their substrates (Fieulaine et al., 2001, 2002; Márquez et al., 2002; Allen et al., 2003). PDRP shares several common features with HprK/Ps. Both belong to the superfamily of P-loop nucleotide-binding protein kinase in which the domain containing the P-loop has an $\alpha/\beta/\alpha$ fold with a central four- or five-stranded parallel β-sheet (Fieulaine et al., 2001, 2002; Márquez et al., 2002; Allen et al., 2003). Additionally, neither HprK/Ps nor PDRP share sequence similarity with eukaryotic Ser/Thr protein kinases, and HprK/Ps are known to catalyze Pi-dependent PPi-generating dephosphorylation. In addition to these resemblances, there are also dramatic differences between them. HprK/Ps use ATP

rather than ADP for phosphorylation. Moreover, PDRP structure is significantly different from that of *M. pneumoniae* HprK/P (PDB ID 1KNX, residues 1–309), with an rmsd of 4.5 Å between 95 corresponding C-alpha atoms. To the best of our knowledge, PDRP may represent the first known plant protein-kinase that utilizes a P-loop for nucleotide substrate binding. The dimeric structure of HprK/P resembles that of PDRP (Fig. 5A), with two separate domains per protomer. The NTD of HprK/P probably provides a platform for protein-protein interactions, while the CTD houses the conserved P-loop that takes part in the enzymatic activities, as we believe to be the case for PDRP (Fieulaine et al., 2001, 2002; Márquez et al., 2002; Allen et al., 2003). Following structural alignment between PDRP and the HprK/P-HPr complex, we could make predictions about the catalytic mechanism of PDRP. There are three key structural parts of PDRP. The first is the P-loop that binds nucleotides or inorganic phosphate. The second is D276 (corresponding to D178 in HprK/P) from the loop between αA and αB (AB-loop) that forms a hydrogen bond with T300 (S162 in HprK/P) may help in forming the metal-binding site, and D277 (D179 in HprK/P) that is bound to P317 (H140 in HprK/P) may protonate or deprotonate the T527 of PPDK to facilitate nucleophilic attack during dephosphorylation and phosphorylation, respectively. Although the distance between these residues is too great in the PDRP structure, the binding of PPDK may alter the conformation of the AB-loop to form the catalytic center. The third is K299 (K161 in HprK/P) from the P-loop and K274 (R245 in HprK/P) from the AB′-loop of the other protomer that together more than likely play an important part in neutralizing the negative charge of the phosphate group and lowering the activation energy during phosphorylation and dephosphorylation (Fig. 5, B and C).

Consistent with an important role in the catalytic mechanism, mutants of D276A/D277A and P317F exhibited a marked decrease in phosphorylation and dephosphorylation activities (Fig. 5D), while mutation of K274 had relatively little effect (Fig. 5D). This may be because PDRP has another residue (K299) to neutralize the negative charge of the phosphate group. Indeed, both of these residues are conserved in PDRP from different species (Supplemental Fig. S1), and circular dichroism (CD) experiments confirmed that the mutants were correctly folded and did not differ conformationally from the wild type (Supplemental Fig. S4). The combined structural and functional studies strongly suggest that PDRP contains a single active site that catalyzes both phosphorylation and dephosphorylation.

DISCUSSION

Since the discovery of the key role of PDRP in C_4 photosynthesis, further studies have proven problematic due to difficulties with protein purification (Ashton et al., 1984; Burnell and Hatch, 1985). Extensive homology searches showed that PDRP shares no sequence similarity with other protein kinases or phosphatases (Chastain et al., 2008). Although Astley et al. (2011) have speculated the active site of Arabidopsis PDRP1 (AtRP1) through the site-directed mutagenesis work of the conserved residues, and Bartlett et al. (2012) have identified the critical residues of *E. coli* PSRP involved

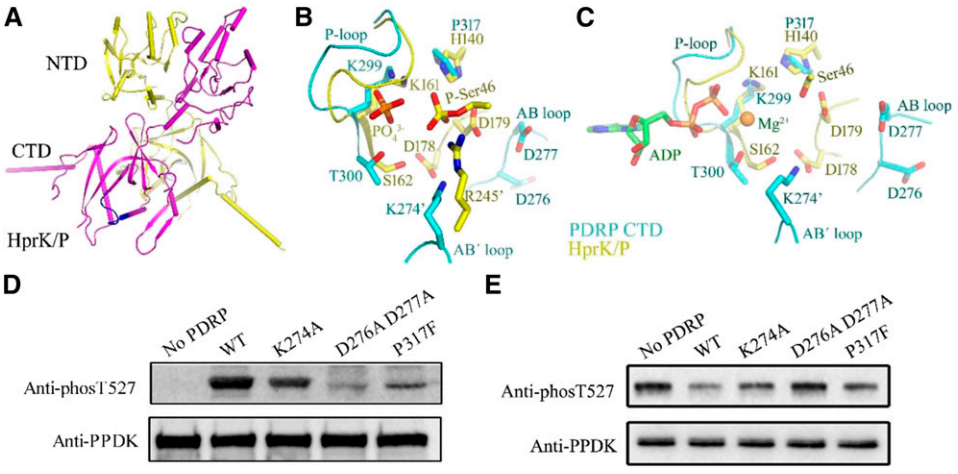

Figure 5. Structural superimposition PDRP onto HprK/P reveals the catalytic mechanism. A, The overall dimeric structure of *M. pneumoniae* HprK/P (PDB ID 1KNX; Allen et al., 2003). The P-loop in the CTD of HprK/P is colored blue. B, Detailed residues involved in the pyrophosphorylase mechanism of PDRP. C, Detailed residues involved in the kinase mechanism of PDRP. Resembling HprK-P-Ser-HPr (PDB ID 1KKM; yellow; Fieulaine et al., 2002) in the dephosphorylation and HprK-Ser-HPr (PDB ID 1KKL; yellow; Fieulaine et al., 2002) in the phosphorylation reaction. PDRP contains three separate regions for the catalytic mechanism: P-loop, Asp-276 and Asp-277 of the AB-loop, and Lys-274 from AB′-loop of the other protomer. The ADP (sticks) and Mg^{2+} (orange sphere) are modeled from shikimate kinase (PDB ID 1L4Y; Gu et al., 2002). D, Immuno-based assays of the in vitro kinase (left) and pyrophosphorylase (right) experiments.

in the enzymatic activities, there has been a lack of detailed structural and mechanism analyses of PDRP until now.

Here we have solved the crystal structure of PDRP, revealing a structure consisting of two separate domains. Despite the structural similarity between the two domains, enzymatic assays showed that the CTD alone is sufficient for both phosphorylation and dephosphorylation activities, and the insufficient limited space between the P-loop, K-loop, and βB may explain the selectivity for ADP, not ATP (Fig. 4B). Moreover, PDRP does not share any of the sequence motifs of the three major protein phosphatase families that depend on metal ions to activate a water molecule or Asp to initiate a nucleophilic attack on the phosphorous atom to generate Pi (Shi, 2009). Structural alignment of PDRP and HprK/P demonstrated a striking resemblance, and both proteins share the conserved sequence motifs consistent with a Pi-dependent, PPi-forming dephosphorylation catalytic mechanism (Fig. 5B). So PDRP may be a new structure of plant pyrophosphorylase. Altogether, we unraveled the details of the catalytic mechanism and provided insights into the evolutionary relationships with other bifunctional enzymes by means of the structural analyses.

In the recent research, Astley et al. (2011) mutated 21 conserved residues in AtRP1 and detected the enzymatic activities of all the mutants on PPDK, then proposed the important residues involved in the active site of AtRP1 (Astley et al., 2011). Through the sequence alignment of PDRPs of plants (Supplemental Fig. S1) and the analyses of maize PDRP structure, we can clearly explain the mechanism of these site-directed mutageneses. The mutations on the conserved residues of the P-loop, AB-loop, and CTD resulted in a decrease of enzymatic activities, while mutants of the putative P-loop of NTD had no effect on the enzymatic activities, in agreement with our conclusion that the NTD of PDRP is not one of the active sites.

In fact, this reversible phosphorylation of PPDK by PDRP was already in place even in the bacteria (Chastain et al., 2011). A sequence alignment of PDRPs of plants and the PSRP of *E. coli* (Supplemental Fig. S1) shows that most residues involved in our proposed catalytic mechanism are highly conserved throughout plants and bacteria, revealing that PSRP of *E. coli* is also a bifunctional ADP-dependent kinase and Pi-dependent pyrophosphorylase, which Burnell (Burnell, 2010) had shown previously. Bartlett et al. (2012) mutated 26 conserved residues in PSRP of *E. coli* and detected the enzymatic activities of all the mutants on PPDK, then proposed that the region identified as a P-loop and residues located at the C-terminal region were important for the binding of ADP and Pi (Bartlett et al., 2012). As with the mutants in AtRP1, the mutations of the NTD did not alter the enzymatic activities, while mutations within the highly conserved P-loop and CTD in PSRP caused a decrease of both enzymatic activities.

Beyond that, residue R350 in maize PDRP (R329 in AtRP1), belonging to the lid-like domain, is important in closing and securing the nucleotide or phosphate groups near the P-loop during the enzymatic activities. We proposed that mutation of R350 would greatly affect the enzymatic activities of maize PDRP. The R329M mutant in AtRP1 brought about a complete loss of enzymatic activities and fit precisely the structure function model and catalytic mechanism proposed by ours (Fig. 4B). Moreover, corresponding to the central region of AtRP1 (residues between D252 and R329; Astley et al., 2011), residues K274 to Y367 of maize PDRP that contain the P-loop, AB-loop, and lid-like domain may directly participate in the interaction and catalysis of PPDK regulation. In addition, we have conjectured that the NTD may function as an allosteric effector that acts to modify the enzymatic activity of maize PDRP and mediate protein-protein interactions with PPDK from the DALI hits of the NTD search, and the structural homology between the NTD and CTD (Fig. 2C) shows that both of them may participate in the PDRP:PPDK interaction.

For the site-directed mutagenesis studies of AtRP1 or PSRP of *E. coli*, they are all compatible with the experimental results of maize PDRP in this study. And through the structural analyses of maize PDRP, we can have a clear understanding of the specific mechanism of these mutants. Therefore, proteins of the DUF 299 gene family may share the same catalytic mechanism for reversible phosphorylation of the substrate PPDK or PEPS.

In summary, we determined the crystal structure for maize PDRP, the first such structure for a DUF299 enzyme family. The structure represents our understanding of a new mechanistic class of protein kinases and pyrophosphorylases and paves the way for future studies to address the evolutionary relationships between PSRP, PDRP, and other bifunctional protein kinase-phosphatases. Structural alignment and in vitro enzymatic assays confirmed that both phosphorylation and dephosphorylation activities occur in the same active site, which answers a long-standing question. Moreover, the interesting structural features of the NTD may be exploited for the development of selective activators or inhibitors to regulate the interaction between PDRP and PPDK and hence photosynthesis.

MATERIALS AND METHODS

Protein Expression and Purification

DNA fragments encoding the wild type (residues 42–426, without the N-terminal 41 residues of the predicted chloroplastic targeting sequence; Burnell and Chastain, 2006), and the corresponding mutants of PDRP were inserted into pMCSG7 vector by ligation independent cloning as well as the NTD (residues 42–256) and the CTD (residues 257–426) fragments. The final clones were verified by DNA sequencing. All of the recombinant plasmids were transformed into *Escherichia coli* strain BL21 (DE3) RIL cells. Cells were then grown in LB at 37°C until OD_{600} reached 0.6 to 0.8 and induced overnight at 18°C by adding 0.2 mM Isopropyl β-D-Thiogalactoside. The cultures were harvested by centrifuging at 4000*g* for 10 min, and the cell pellets resuspended in lysis buffer (20 mM Tris, pH 8.0, 500 mM NaCl, and 2% Dioxane) replenished with 0.1% (v/v) Triton X-100 and 1 mM PMSF (Invitrogen). After cell lysis by sonication and centrifugation at 20,000*g* for 10 min, the supernatant was applied to profinity

IMAC resins (Bio-Rad) with 20 mM imidazole. The column was washed with lysis buffer containing 20 mM imidazole and the protein eluted with lysis buffer containing 200 mM imidazole. The purity of the eluted protein was examined by SDS-PAGE. The protein was concentrated to 10 mg/mL for crystallization.

Crystallization and Data Collection

Initial screening was performed at 18°C and 4°C. Crystals appeared in the reservoir solution of 10% PEG 20000, 0.1 M Bicine, pH 9.0, and 2% Dioxane at 4°C. The diffraction ability of these crystals was poor. The diffraction qualities were not improved after extensive optimization of crystallization conditions or various postcrystallization treatments such as annealing and dehydration. After rescreening by adding different additives, high-quality crystals were finally obtained in the optimized well solution made up of 1.0 M K/Na tartrate 0.1 M MOPS, pH 8.0, 1% Dioxane, 1 mM AMP, and 2 mM Mg^{2+}. All the crystals were transferred to a cryo-buffer (supplemented with 20% ethylene glycol) and were snap frozen in liquid nitrogen before data collection. Data were indexed, integrated, and scaled with the HKL2000 (Winn et al., 2011). Data collection and processing statistics are shown in Supplemental Table S1.

To solve the structure, the apo-PDRP crystals were soaked in the crystallization well solution with 10 mM Ethylmercurithiosalicylic acid and then transferred to a cryo-buffer and were snap frozen in liquid nitrogen before data collection. Strong anomalous signal data were collected at 100 K.

Structure Determination and Refinement

The heavy atom positions in the Hg-derived PDRP crystal of *P*432 space group were determined using the program SHARP with single-wavelength anomalous diffraction (Vonrhein et al., 2007). Two initial Hg sites were refined and the phases were generated. The preliminary outcome R_{work}/R_{free} values were 47%/47% with 17 secondary structural fragments set up by 170 residues. A crude partial model was built manually in the program COOT (Emsley and Cowtan, 2004). The structure was completed in alternating cycles of manual model building (in COOT) and restrained refinement (in refmac5; Murshudov et al., 2011), and the final R_{work}/R_{free} is 21.9%/3.4%. All figures in this article displaying molecular structure were made using PYMOL (Schrödinger, 2010).

In Vitro PDRP Protein Phosphorylation and Dephosphorylation Assays

The PDRP protein kinase activities were assayed as modified from a previously described method (Chastain et al., 2008). Purified recombinant 70 μg His-PPDK and 15 μg His-PDRP were incubated with 1 mL reaction mixture consisting of 50 mM Bicine, pH 8.3, 10 mM $MgCl_2$, 5 mM DTT, 1 mg/mL BSA, 1 mM ADP, and 0.2 mM ATP. After 30 min at 30°C, 20 μL of the PDRP protein kinase reaction was heated at 100°C to denature the proteins.

The PDRP protein dephosphorylation assays was executed by the addition of 10 μg purified recombinant PDRP to a 200-μL reaction mixture consisting of 5 μg recombinant purified phosphor-PPDK, 50 mM HEPES, pH 8.0, 10 mM $MgCl_2$, 0.1 mM EDTA, 10 mM $NaHCO_3$, 5 mM NH_4Cl, 1 mM Glc 6-phosphate disodium, 10 mM DTT, 2.5 mM KH_2PO_4, and 2.5 mM K_3PO_4. After 30 min at 30°C, 40 μL of the PDRP protein pyrophosphorylase reaction was heated at 100°C to denature the proteins. All the protein samples were detected by anti-PDRP, anti-PPDK, or antiphospho-T527-PPDK antibodies.

Size-Exclusion Chromatography and Analytical Ultracentrifugation

The size-exclusion chromatography experiments were performed in Superdex-200 (GE Healthcare) using gel-filtration buffer (20 mM Tris, pH range of 7.5–8.3, 500 mM NaCl, 2% Dioxane) for purified recombinant HIS-PDRP. Peak fractions were collected and analyzed by SDS-PAGE.

SV experiments were performed in a Beckman/Coulter XL-I analytical ultracentrifuge using double-sector or six-channel centerpieces and sapphire windows. An additional protein purification step applied to size-exclusion chromatography in buffer containing 20 mM Tris, pH 8.0, 150 mM NaCl was performed before experiments. SV experiments were conducted at 42,000 rpm and 20°C using interference detection and double-sector cells loaded at approximate 0.1 mM PDRP. The buffer composition (density and viscosity) and protein partial specific volume (V-bar) were obtained using the program SEDNTERP. The SV data were analyzed using the SEDFIT and SEDPHAT programs (Schuck, 2000, 2003).

CD Analysis

The CD spectroscopy analysis was measured at the 4B8 beamline in the Beijing synchrotron radiation facility. Spectra were collected at 1-nm intervals over the wavelength ranging from 260 to 180 nm in a 0.005-cm optical path length at 25°C. A pure solution baseline collected with the same cell was subtracted, and all spectra data were processed using the CD tool software (Lees et al., 2004). Protein samples were prepared at a concentration of about 1 mg/mL. The machine unit (mdeg) was converted into the per residue molar absorption unit, delta epsilon ($\Delta\varepsilon$) in M/cm, by normalization with respect to polypeptide concentration and path length.

Accession Numbers

Coordinates and structure factors have been deposited in the Protein Data Bank under accession codes 5D0N and 5D1F.

Supplemental Data

The following supplemental materials are available.

Supplemental Figure S1. Secondary structure alignment of PDRP from different species.

Supplemental Figure S2. Size exclusion chromatography and analytical ultracentrifugation of PDRP.

Supplemental Figure S3. The temperature B-factors representation of PDRP structure (A) and the two disulfide bonds (B).

Supplemental Figure S4. The circular dichroism data of PDRP wild type and various mutants.

Supplemental Table S1. Data collection and refinement statistics of PDRP*

Supplemental Movies S1 and S2. There are two supplementary movies on the Web site: one for PDRP monomer, one for PDRP dimer.

ACKNOWLEDGMENTS

We thank the staff at the beamline BL17B at Shanghai Synchrotron Radiation Facility, beamline BL5A of at Photon Factory (Tsukuba, Japan), and the beamline 1W2B at the Beijing Synchrotron Radiation Facility for the excellent technical assistance during data collection.

Received November 3, 2015; accepted November 25, 2015; published November 30, 2015.

LITERATURE CITED

Allen GS, Steinhauer K, Hillen W, Stülke J, Brennan RG (2003) Crystal structure of HPr kinase/phosphatase from *Mycoplasma pneumoniae.* J Mol Biol **326:** 1203–1217

Ashton AR, Burnell JN, Hatch MD (1984) Regulation of C_4 photosynthesis: inactivation of pyruvate, Pi dikinase by ADP-dependent phosphorylation and activation by phosphorolysis. Arch Biochem Biophys **230:** 492–503

Astley HM, Parsley K, Aubry S, Chastain CJ, Burnell JN, Webb ME, Hibberd JM (2011) The pyruvate, orthophosphate dikinase regulatory proteins of *Arabidopsis* are both bifunctional and interact with the catalytic and nucleotide-binding domains of pyruvate, orthophosphate dikinase. Plant J **68:** 1070–1080

Bartlett S, Seeliger J, Burnell JN (2012) Identification of critical residues in the bifunctional phosphorenolpyruvate synthetase kinase/phosphotransferase of *Escherichia coli.* Curr Top Biochem Res **14:** 77–83

Burnell JN (2010) Cloning and characterization of *Escherichia coli* DUF299: a bifunctional ADP-dependent kinase–Pi-dependent pyrophosphorylase from bacteria. BMC Biochem **11:** 1

Burnell JN, Chastain CJ (2006) Cloning and expression of maize-leaf pyruvate, Pi dikinase regulatory protein gene. Biochem Biophys Res Commun **345:** 675–680

Burnell JN, Hatch MD (1983) Dark-light regulation of pyruvate, Pi dikinase in C_4 plants: evidence that the same protein catalyses activation and inactivation. Biochem Biophys Res Commun **111:** 288–293

Burnell JN, Hatch MD (1985) Regulation of C_4 photosynthesis: purification and properties of the protein catalyzing ADP-mediated inactivation and Pi-mediated activation of pyruvate,Pi dikinase. Arch Biochem Biophys **237:** 490–503

Burnell JN, Hatch MD (1986) Activation and inactivation of an enzyme catalyzed by a single, bifunctional protein: a new example and why. Arch Biochem Biophys **245:** 297–304

Chastain CJ, Botschner M, Harrington GE, Thompson BJ, Mills SE, Sarath G, Chollet R (2000) Further analysis of maize $C(_4)$ pyruvate, orthophosphate dikinase phosphorylation by its bifunctional regulatory protein using selective substitutions of the regulatory Thr-456 and catalytic His-458 residues. Arch Biochem Biophys **375:** 165–170

Chastain CJ, Failing CJ, Manandhar L, Zimmerman MA, Lakner MM, Nguyen TH (2011) Functional evolution of $C(_4)$ pyruvate, orthophosphate dikinase. J Exp Bot **62:** 3083–3091

Chastain CJ, Xu W, Parsley K, Sarath G, Hibberd JM, Chollet R (2008) The pyruvate, orthophosphate dikinase regulatory proteins of *Arabidopsis* possess a novel, unprecedented Ser/Thr protein kinase primary structure. Plant J **53:** 854–863

Chen L, Dürr KL, Gouaux E (2014a) X-ray structures of AMPA receptor-cone snail toxin complexes illuminate activation mechanism. Science **345:** 1021–1026

Chen YB, Lu TC, Wang HX, Shen J, Bu TT, Chao Q, Gao ZF, Zhu XG, Wang YF, Wang BC (2014b) Posttranslational modification of maize chloroplast pyruvate orthophosphate dikinase reveals the precise regulatory mechanism of its enzymatic activity. Plant Physiol **165:** 534–549

Dürr KL, Chen L, Stein RA, De Zorzi R, Folea IM, Walz T, Mchaourab HS, Gouaux E (2014) Structure and dynamics of AMPA receptor GluA2 in resting, pre-open, and desensitized states. Cell **158:** 778–792

Edwards GE, Nakamoto H, Burnell JN, Hatch MD (1985) Pyruvate, Pi dikinase and NADP-malate dehydrogenase in C_4 photosynthesis: properties and mechanism of light/dark regulation. Annu Rev Plant Physiol **36:** 255–286

Emanuelsson O, Nielsen H, von Heijne G (1999) ChloroP, a neural network-based method for predicting chloroplast transit peptides and their cleavage sites. Protein Sci **8:** 978–984

Emsley P, Cowtan K (2004) Coot: model-building tools for molecular graphics. Acta Crystallogr D Biol Crystallogr **60:** 2126–2132

Fieulaine S, Morera S, Poncet S, Mijakovic I, Galinier A, Janin J, Deutscher J, Nessler S (2002) X-ray structure of a bifunctional protein kinase in complex with its protein substrate HPr. Proc Natl Acad Sci USA **99:** 13437–13441

Fieulaine S, Morera S, Poncet S, Monedero V, Gueguen-Chaignon V, Galinier A, Janin J, Deutscher J, Nessler S (2001) X-ray structure of HPr kinase: a bacterial protein kinase with a P-loop nucleotide-binding domain. EMBO J **20:** 3917–3927

Gan J, Gu Y, Li Y, Yan H, Ji X (2006) Crystal structure of *Mycobacterium tuberculosis* shikimate kinase in complex with shikimic acid and an ATP analogue. Biochemistry **45:** 8539–8545

Gu Y, Reshetnikova L, Li Y, Wu Y, Yan H, Singh S, Ji X (2002) Crystal structure of shikimate kinase from *Mycobacterium tuberculosis* reveals the dynamic role of the LID domain in catalysis. J Mol Biol **319:** 779–789

Hatch MD, Slack CR (1969) Studies on the mechanism of activation and inactivation of pyruvate, phosphate dikinase. A possible regulatory role for the enzyme in the C_4 dicarboxylic acid pathway of photosynthesis. Biochem J **112:** 549–558

Lees JG, Smith BR, Wien F, Miles AJ, Wallace BA (2004) CDtool-an integrated software package for circular dichroism spectroscopic data processing, analysis, and archiving. Anal Biochem **332:** 285–289

Márquez JA, Hasenbein S, Koch B, Fieulaine S, Nessler S, Russell RB, Hengstenberg W, Scheffzek K (2002) Structure of the full-length HPr kinase/phosphatase from *Staphylococcus xylosus* at 1.95 A resolution: mimicking the product/substrate of the phospho transfer reactions. Proc Natl Acad Sci USA **99:** 3458–3463

Murshudov GN, Kubák P, Lebedev AA, Pannu NS, Steiner RA, Nicholls RA, Winn MD, Long F, Vagin AA (2011) REFMAC5 for the refinement of macromolecular crystal structures. Acta Crystallogr D Biol Crystallogr **67:** 355–367

Scheeff ED, Bourne PE (2005) Structural evolution of the protein kinase-like superfamily. PLOS Comput Biol **1:** e49

Schrödinger LLC (2010) The PyMOL Molecular Graphics System, Version 1.3. Schrödinger LLC, New York

Schuck P (2000) Size-distribution analysis of macromolecules by sedimentation velocity ultracentrifugation and lamm equation modeling. Biophys J **78:** 1606–1619

Schuck P (2003) On the analysis of protein self-association by sedimentation velocity analytical ultracentrifugation. Anal Biochem **320:** 104–124

Shi Y (2009) Serine/threonine phosphatases: mechanism through structure. Cell **139:** 468–484

Vonrhein C, Blanc E, Roversi P, Bricogne G (2007) Automated structure solution with autoSHARP. Methods Mol Biol **364:** 215–230

Winn MD, Ballard CC, Cowtan KD, Dodson EJ, Emsley P, Evans PR, Keegan RM, Krissinel EB, Leslie AG, McCoy A, et al (2011) Overview of the CCP4 suite and current developments. Acta Crystallogr D Biol Crystallogr **67:** 235–242